

FAST ACOUSTIC IMAGING WITH SEPARABLE ARRAYS**Bruno S. Masiero****César S. B. Arroyo****Vítor H. Nascimento**

Laboratório de Processamento de Sinais da Escola Politécnica da Universidade de São Paulo.

Av. Prof. Luciano Gualberto, trav. 3, 158. São Paulo, 05508-900

{masiero,vitor}@lps.usp.br

Flávio P. Ribeiro

Microsoft Corporation Applied Sciences Group.

flaviopr@microsoft.com

Abstract. We compare acoustic images obtained from actual measurements using a 49-microphone array with separable geometry. Images were obtained using four different algorithms: delay-and-sum beamforming (DAS), DAMAS2, and two regularized least-squares methods, the first using ℓ_1 regularization, the second using total variation (TV) regularization. All algorithms were accelerated using the Kronecker array transform (KAT), a method that is applicable for arrays whose microphones are positioned in a separable, possibly non-uniform grid. We also compare results obtained with and without microphone calibration, verifying the influence of correct calibration. The results show that regularized least-squares methods tend to provide the best results.

Keywords: acoustic imaging, fast transform, array processing, sparse reconstruction

1. INTRODUCTION

Microphone arrays are commonly used to estimate sound levels arriving from different directions. An *acoustic image* is generated when the estimated acoustic levels are coded into a colormap, generating an image of sound level as a function of direction of arrival. Acoustic images are commonly associated with the problem of detecting and characterizing acoustic sources and can be superimposed over photographs to help identify unknown sound sources or compare the relative sound power emitted by a set of sound sources.

Traditional acoustic imaging techniques, such as the delay-and-sum (DAS) beamformer, will pass the signals acquired with the microphone array through a spatial filter, matched to both the array geometry and the source directions. This filter acts as a two-dimensional window function convolved with the impinging sound field (Johnson and Dudgeon, 1993). Microphone arrays usually have a reduced number of sensors, which results in a window function—the point spread function (PSF)—with a wide beamwidth and, consequently, in a smeared acoustic image.

Many methods have been proposed to increase image resolution without altering the number of microphones, either by applying deconvolution techniques to eliminate the aforementioned convolution effect (Wang et al., 2004; Dougherty, 2005; Ehrenfried and Koop, 2007); or using regularized optimization (Yardibi et al., 2008). These methods have in common the fact that they are based on iterative approaches, requiring elevated computational load for their solution. To counter this situation and allow the practical use of more advanced acoustic imaging techniques, the Kronecker Array Transform (KAT) was recently developed to provide significant reduction of the computational cost for array processing, with the single restriction that the microphones should be distributed in a separable geometry (Ribeiro and Nascimento 2011a)

Ribeiro and Nascimento (2011b) discussed that, even though microphone arrays with separable geometry are not optimal for the use with the DAS beamformer, images obtained from an array with separable geometry and KAT accelerated iterative algorithms showed improved results when compared to images obtained with DAS beamformer and an array optimized for that method. These results motivated the development of an array with 64 microphones distributed in a separable geometry. The array was built with MEMS microphones to reduce costs and increase placement precision. The microphone signals are acquired and downsampled via an FPGA connected to a computer used for post-processing.

All array processing methods discussed in this manuscript assume that the relative position of the sensors is known, and, furthermore, that all sensors have the same sensitivity and directivity. Note that any discrepancy in microphone positioning or gain will result in a different PSF function, mismatched to the designed spatial filters, and consequently leading to distortions at the estimated acoustic image (Khong and Brookes, 2007).

In practical applications exact positioning of the microphones cannot always be guaranteed, in the same manner that microphones might present a variation in their responses. The influence of these imperfections can be countered by the calibration of the array. Several techniques have been proposed to calibrate the position and sensitivity of the microphones, but they all require exact knowledge of the reference source's position (Xiao, Shao, and Peng 2007; Valente et al. 2010). *Blind* calibration algorithms can be used in the attempt to conduct calibration without prior

knowledge of the reference sources (Weiss and Friedlander, 1990; Flanagan and Bell, 2001). These methods first estimate the position of the reference sources using some “direction-of-arrival” (DOA) algorithm and assuming the nominal array configuration. Next, assuming correct DOA estimate, the array parameters are estimated. These two steps are repeated iteratively until the estimate converge, which can be viewed as a joint estimation problem using “group alternating maximization” (van Trees, 2002).

In this paper we will first present the imaging algorithms used and how they can be accelerated with the KAT. We then discuss the calibration efforts required before using the array and finally we present experimental results. Two miniature loudspeakers are used to mimic a point source and provide a stable sound field for the measurements conducted at a dry (but not anechoic) room.

2. IMAGE RECONSTRUCTION METHODS

The KAT optimization presented in (Ribeiro and Nascimento, 2011a) requires Cartesian (not necessarily uniform) parameterization in U-space and far-field approximations.

We define \mathbf{u}_m the look direction of the planar array, which lies in a unit half-sphere with elevation angle ϕ and azimuth angle θ . The look direction can be parameterized in the U-space as follows

$$\mathbf{u}_m = \begin{bmatrix} \sin \phi \cos \theta \\ \cos \phi \cos \theta \\ \sin \theta \end{bmatrix} = \begin{bmatrix} u_x \\ u_y \\ \sqrt{1 - u_x^2 - u_y^2} \end{bmatrix}, \quad (1)$$

for $u \in [-1, 1]$ and $u_x^2 + u_y^2 \leq 1$.

Assuming all sources lie in the far-field, we define the microphone array output vector (transformed using the discrete Fourier transform (DFT) using an adequate window length) as

$$\mathbf{x}(\omega_k) = \mathbf{V}(\omega_k) \mathbf{f}(\omega_k) + \boldsymbol{\eta}(\omega_k), \quad (2)$$

where $\mathbf{V}(\omega_k) = [\mathbf{v}(\mathbf{u}_0, \omega_k) \quad \mathbf{v}(\mathbf{u}_1, \omega_k) \quad \cdots \quad \mathbf{v}(\mathbf{u}_{M-1}, \omega_k)]$ is the matrix formed by the concatenation of the manifold vectors for each look direction, $\mathbf{f}(\omega_k)$ is the frequency domain signal vector and $\boldsymbol{\eta}(\omega_k)$ is the frequency domain noise vector. We further define the array’s narrow-band cross spectral matrix as

$$\mathbf{R}_x(\omega_k) = E\{\mathbf{x}(\omega_k)\mathbf{x}^H(\omega_k)\}. \quad (3)$$

For the remaining of this manuscript we omit ω_k in order to simplify the notation.

2.1 Delay and sum beamforming

The delay and sum imaging is implemented as a spatial filter, i.e., a weighted sum of the array signals. The weights for the DAS beamformer are given by $\mathbf{w}(\mathbf{u}_m) = 1/M \mathbf{v}(\mathbf{u}_m) = \mathbf{v}(\mathbf{u}_m) / (\mathbf{v}^H(\mathbf{u}_m)\mathbf{v}(\mathbf{u}_m))$ (Krim and Viberg, 1996) and the acoustic imaged is estimated from

$$\hat{Y}_m = \frac{\mathbf{v}^H(\mathbf{u}_m)\mathbf{R}_x\mathbf{v}(\mathbf{u}_m)}{[\mathbf{v}^H(\mathbf{u}_m)\mathbf{v}(\mathbf{u}_m)]^2}. \quad (4)$$

Ribeiro and Nascimento (2011b) demonstrate that eq. (4) can be rewritten as

$$\hat{\mathbf{y}} = \frac{1}{M^2} \mathbf{A}^H \text{vec}\{\mathbf{R}_x\}, \quad (5)$$

where $\hat{\mathbf{y}} = [\hat{Y}_0 \quad \hat{Y}_1 \quad \cdots \quad \hat{Y}_M]$ is a vector whose elements are the acoustic image pixels. The DAS can now be implemented with the adjoint KAT (Ribeiro and Nascimento, 2011b).¹

¹ Optimal beamforming algorithms (van Trees, 2002) can also profit from the KAT, however they will not be evaluated in this manuscript.

2.2 DAMAS2

It can be verified that the acoustic image obtained with the DAS beamformer is the convolution between the arrays PSF and the “clean” image. DAMAS2 is a state of the art method, developed for aeroacoustic imaging, to eliminate the convolution effect. Defining $\hat{\mathbf{Y}}$ as the image obtained with the DAS beamformer and $\hat{\mathbf{Y}}$ as the clean image, the DAMAS2 iterative procedure is defined as

$$\hat{\mathbf{Y}}^{(k+1)} = \max \left\{ \hat{\mathbf{Y}}^{(k)} - \frac{1}{a} [\hat{\mathbf{Y}} - \mathbf{PSF} * \hat{\mathbf{Y}}^{(k)}], \mathbf{0} \right\}, \quad (6)$$

where $*$ denotes 2-D convolution, $\hat{\mathbf{Y}}^{(k)}$ is the reconstructed image at iteration k with $\hat{\mathbf{Y}}^{(0)} = \mathbf{0}$. \mathbf{PSF} is the discretized PSF, $a = \sum_{i,j} |\mathbf{PSF}|_{i,j}$, and $\max\{\cdot, \cdot\}$ returns the pointwise maximum.

Ribeiro and Nascimento (2011b) show that $\mathbf{PSF} * \hat{\mathbf{Y}} = \mathbf{A}^H \mathbf{A} \hat{\mathbf{y}}^{(k)}$, where $\mathbf{A}^H \mathbf{A}$ can be implemented with the fast direct-adjoint KAT and since the convolutions are the bottleneck for calculating DAMAS2, a significant performance improvement can be obtained when substituting the convolution by the KAT.

2.3 ℓ_1 -regularized least squares

DAMAS2 does not use any regularization other than forcing pointwise non-negativity to guarantee strictly positive power estimates, i.e., it does not incorporate a prior knowledge. Prior models of the source distribution can be incorporated as constraints to the linear system of equations obtained by substituting eq. (2) in eq. (3). If we assume that only a small number of U-space points have radiating sources, then a sparse prior model can be applied resulting in the basis pursuit problem

$$\underset{\hat{\mathbf{y}}}{\operatorname{argmin}} \|\hat{\mathbf{y}}\|_1 \text{ subject to } \|\operatorname{vec}\{\mathbf{R}_x\} - \mathbf{A}\hat{\mathbf{y}}\|_2 \leq \sigma, \quad (7)$$

where σ^2 is the white noise power.

2.4 Total variation regularized least squares

For situations where the sparsity prior is not adequate another possibility is to apply the total variation (TV) regularization, which tends to privilege smooth solutions with small amounts of noise.

The isotropic total variation norm is defined as $\|\mathbf{Y}\|_{TV} = \sum_{i,j} \sqrt{[\nabla_x \mathbf{Y}]_{i,j}^2 + [\nabla_y \mathbf{Y}]_{i,j}^2}$, where ∇_x and ∇_y are the first difference operators along the x and y dimensions and the TV optimization problem is

$$\begin{aligned} & \underset{\hat{\mathbf{y}}}{\operatorname{argmin}} \|\hat{\mathbf{y}}\|_{TV} + \mu \|\operatorname{vec}\{\mathbf{R}_x\} - \mathbf{A}\hat{\mathbf{y}}\|_2^2 \\ & \text{subject to } [\hat{\mathbf{Y}}]_{i,j} \geq 0. \end{aligned} \quad (8)$$

This method provides accurate and stable image reconstructions with guaranteed convergence.

3. SEPARABLE MICROPHONE ARRAY

To test the feasibility of the KAT for practical applications a microphone array with separable geometry was designed by Ribeiro (2012). To avoid the use of A/D converters—namely the most expensive component in a standard microphone array—MEMS microphones with integrated 1 bit A/D converters were used. Because of their fabrication methods, MEMS microphones also present lower sensitivity variance when compared to electret microphones. An FPGA Stratix III 3SL150 with 1 GB of DDR3 RAM was used to acquire the microphone signals at 2.4 MHz, downsample them to 48 kHz with 16 bits, and send them to a PC for post-processing. This FPGA can acquire the signal of up to 256 microphones simultaneously.

We designed a planar array with 64 microphones positioned in an 8×8 grid and with horizontal and vertical apertures of 35 cm. Each line and column of the array is chosen to be a nonredundant array with minimum missing lags (Vertatschitsch and Haykin, 1986) as presented in Figure 1.

The presented array was fabricated on a single printed circuit board using reflow soldering, what guarantees precise positioning of the microphones. However, it was verified that the microphones presented considerable variance in sensitivity response, probably caused by some difficulties during the fabrication process, which also resulted in two damaged microphones whose signals had to be discarded. Because the KAT requires a separable geometry, the line and column of sensors containing the damaged microphones had to be discarded, represented by the red lines in Figure 1, so that acoustic images could still be calculated using the KAT, only now using the remaining 7×7 microphone grid.

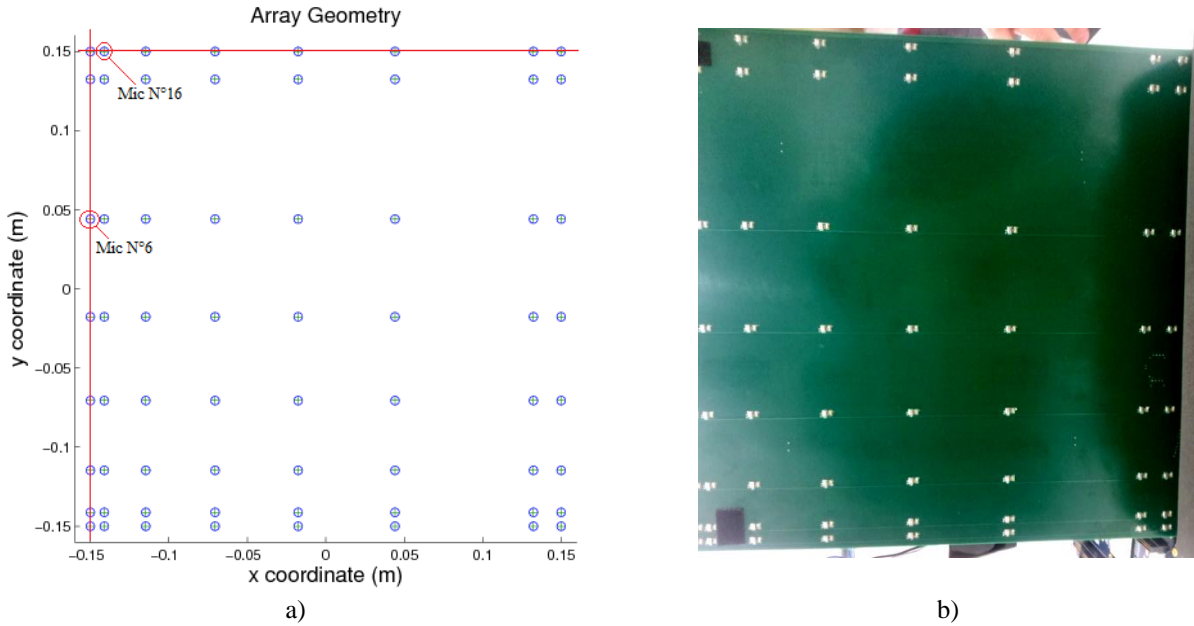


Figure 1. The projected 64-element microphone array with separable geometry. a) Circles represent the microphone positions. The two damaged microphones (#6 and #16) are highlighted as well as the line and column eliminated in post-processing. b) The fabricated PCB with the 64 MEMS microphones.

4. MEASUREMENT SETUP

The measurements presented in the next sections were performed at a studio from the Signal Processing Lab of University of São Paulo. This is a room—measuring 2.91×2.56 m and 2.93 m high—constructed from double wooden panels covered with a 5 cm thick foam material for reduced acoustic reflections while the floor is covered with carpet. At one of the side walls there is a 1 m^2 glass window. For the measurements this window was also covered with the same absorbing material. Therefore the room is clearly not an anechoic space, especially at lower frequencies. Even though this structure does not allow complete isolation from outside noise the studio offers an environment with reduced background noise.

The measurements were performed using two miniature loudspeakers from the manufacturer X-mini. Because of its reduced size, the X-mini II model can be considered a good approximation to an acoustic point source. The loudspeaker has a nominal output power of 2 W and nominal frequency range from 100 Hz to 20 kHz with total harmonic distortion $\text{THD} \leq 1\%$. Both the microphone array and the loudspeakers were placed inside the room using regular microphone stands.

5. MICROPHONE ARRAY CALIBRATION

Even though microphone positioning errors are irrelevant thanks to the array's fabrication process employed, variations in the microphone sensitivity were verified by measuring the acoustic background noise level in a reverberant space, which is not equal to all microphones as would be the case if microphone sensitivity was identical.

An array calibration procedure was then performed at the aforementioned studio. The miniature loudspeaker was placed directly in front of the microphone array at a distance of 2 m. The transfer function between the loudspeaker and each of the array microphones was measured with the ITA-Toolbox using a sine sweep of 2^{16} samples at 48 kHz sampling rate, frequency range from 200 Hz to 24 kHz and a 0.1 s stop margin (Dietrich et al., 2010).

The measured transfer function given by

$$F_m(\omega) = LS(\omega) \cdot G_m(\omega) \cdot MIC_m(\omega) \quad (9)$$

can be decomposed into three components: the loudspeaker frequency response $LS(\omega)$, the transfer function between loudspeaker and microphones described by the Green's function $G_m(\omega)$, and each microphone's own frequency response $MIC_m(\omega)$. We wish to eliminate the first two components to obtain only the microphone's frequency response

(or the relative variation between them). The first step is to divide all measured transfer functions by the transfer function of one microphone chosen as the reference microphone, thus eliminating $LS(\omega)$. However, because the room used for the measurements is not an anechoic space, the reflections present at the measured impulse responses can result in artifacts that will corrupt all further processing. The reflections were eliminated by applying a Tukey time window with 256 samples and 50% taper ratio centered at the start of the impulse to all channels. To eliminate further non-causal artifacts caused by noise at frequencies not excited by the loudspeaker the transfer function division operation was implemented as a minimum phase regularized inversion (Bouchard et al. 2006).

Further on, to eliminate the influence of $G_m(\omega)$ we need to determine the loudspeaker position relative to the microphone array. To do so, the relative time lag between the impulse response of each channel to the reference microphone was calculated applying a PHAT-GCC algorithm to the signals, which were also oversampled by a factor of 32. The obtained time lag information was then fed to a sphere fitting algorithm (MATLAB's `spherefit.m`) that estimates the source position based on a spherical wave propagation model. The obtained results were in good agreement with the actual measurement setup. Knowing the estimated distance d_m from the source to each microphone we can now calculate the Green's function $G_m(\omega) = e^{jk_d m}/d_m$ and eliminate its influence from $F_m(\omega)$, resulting only in $F'_m(\omega) = MIC_m(\omega)/MIC_{REF}(\omega)$, each microphone's sensitivity relative to the reference microphone's sensitivity.

The resulting impulse responses are further time-windowed using a single-sided Tukey window with 48 samples and 50% taper ratio. Calibration is accomplished by convolving the signal at each microphone signal with an FIR filter whose coefficients are obtained from the respective windowed impulse responses obtained above for each channel.

In the next section we compare acoustic images obtained before and after the array's calibration procedure.

6. IMAGING RESULTS

In the following we compare the imaging results obtained using DAS beamformer, DAMAS2, and covariance fitting with ℓ_1 - and TV-regularization. The regularized optimization problems were solved using the SPGL1 toolbox (van den Berg and Friedlander, 2008) for solving Eq. (7) using 200 iterations and $\sigma = 0.01 \|\mathbf{R}_x\|_F$.² For the solution of Eq. (8) we used the TVAL3 toolbox (Li, 2009) using 100 iterations and $\mu = 10^3$. For DAMAS2 we used 1000 iterations. All calculations were made using MATLAB 64 bit running at an Intel Core i7-3770 processor and all algorithms were accelerated using the KAT. The average reconstruction time were as follow: 0.13 s for the DAS beamformer, 1.58 s for the DAMAS2, 1.96 s for the ℓ_1 -regularized reconstruction and 2.46 s for the TV-regularized reconstruction. Even though the KAT is able to accelerate the calculations up to the orders of a thousand times, the time take for reconstruction is still prohibitive for on line monitoring.

The look directions were sampled uniformly in the whole U-space with 256 points in each direction. Note that because of the KAT requirements the algorithms also compute values outside the visible region (i.e., for points with $u_x^2 + u_y^2 > 1$). Ideally, the resulting images should have only small (blue) values outside the visible region. This constitutes a preliminary test of the quality of reconstruction algorithms. In the next figures, the vertical axis represents $u_x \in [-1,1]$ and the horizontal axis represents $u_y \in [-1,1]$. The visible region boundary ($u_x^2 + u_y^2 = 1$) is marked with a black circle.

Below we present the results obtained for different source configurations. In all cases the same sine sweep used at the calibration stage was also used as excitation signal. For every configuration we present the results obtained using each of the discussed imaging methods at two distinct frequencies and both with and without calibration of the microphone array.

6.1 One loudspeaker 1.5 m in front of the microphone array

We first place the sound source 1.5 m in front of the center of the microphone array. The observed images should ideally depict only a small red circle in the center of an otherwise blue background. Figure 2 shows the acoustic image obtained at 1 kHz. This example shows the deficiencies of DAS beamformer, the images are smeared and have artifacts due to sidelobes. DAMAS2 produces very good results, with small artifacts on the edges. ℓ_1 -regularized reconstruction shows an image with some artifacts while TV-regularization produces that best resembles the expected image for this setup, only with some artifacts at the border of the visible range.

Figure 3 presents reconstruction results for a frequency of 5 kHz. For this frequency the ℓ_1 -regularized reconstruction algorithm did not converge to a solution and therefore we do not present an image for this method. At this frequency we clearly see the presence of sidelobes from the array's PSF at the image obtained with DAS. DAMAS2 and TV-regularization considerably reduced the presence of these sidelobes in their final images, even though they could not be completely removed. Especially in the images obtained with DAS and TV-regularization we are able to verify the influence of calibration; on the first image the sidelobe structure became more regular, as would be expected, and on the second image we notice the presence of fewer artifacts at the image obtained from calibrated result.

² $\|\cdot\|_F$ is the Frobenius norm.

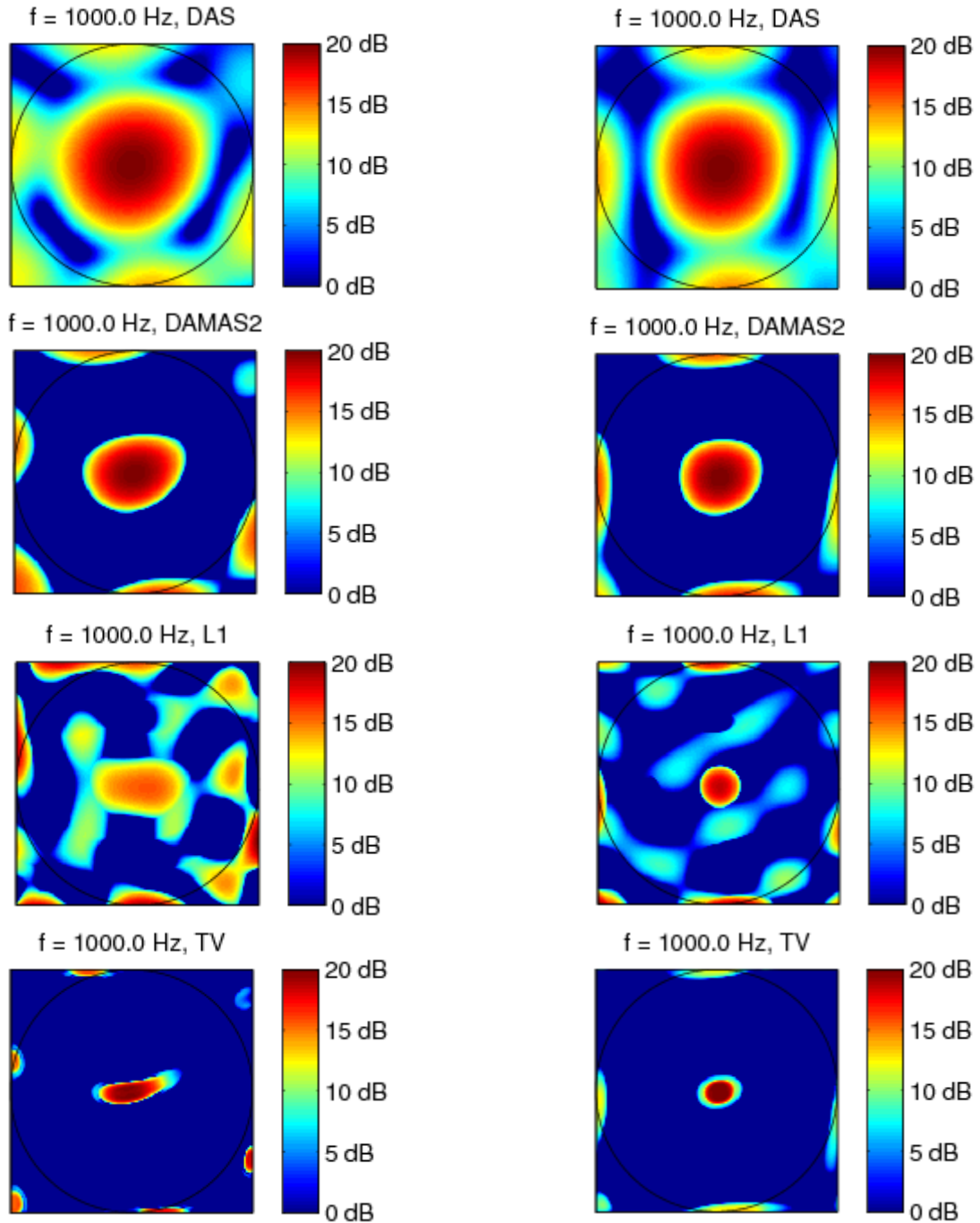


Figure 2. Acoustic images at 1 kHz obtained from microphone array measurements from a miniature loudspeaker positioned 1.5 m in front of the array calculated with DAS beamformer (1st line), DAMAS2 (2nd line), ℓ_1 -regularized reconstruction (3rd line), and TV regularized reconstruction (4th line). First column shows reconstruction without calibration, and second column shows reconstruction with calibration.

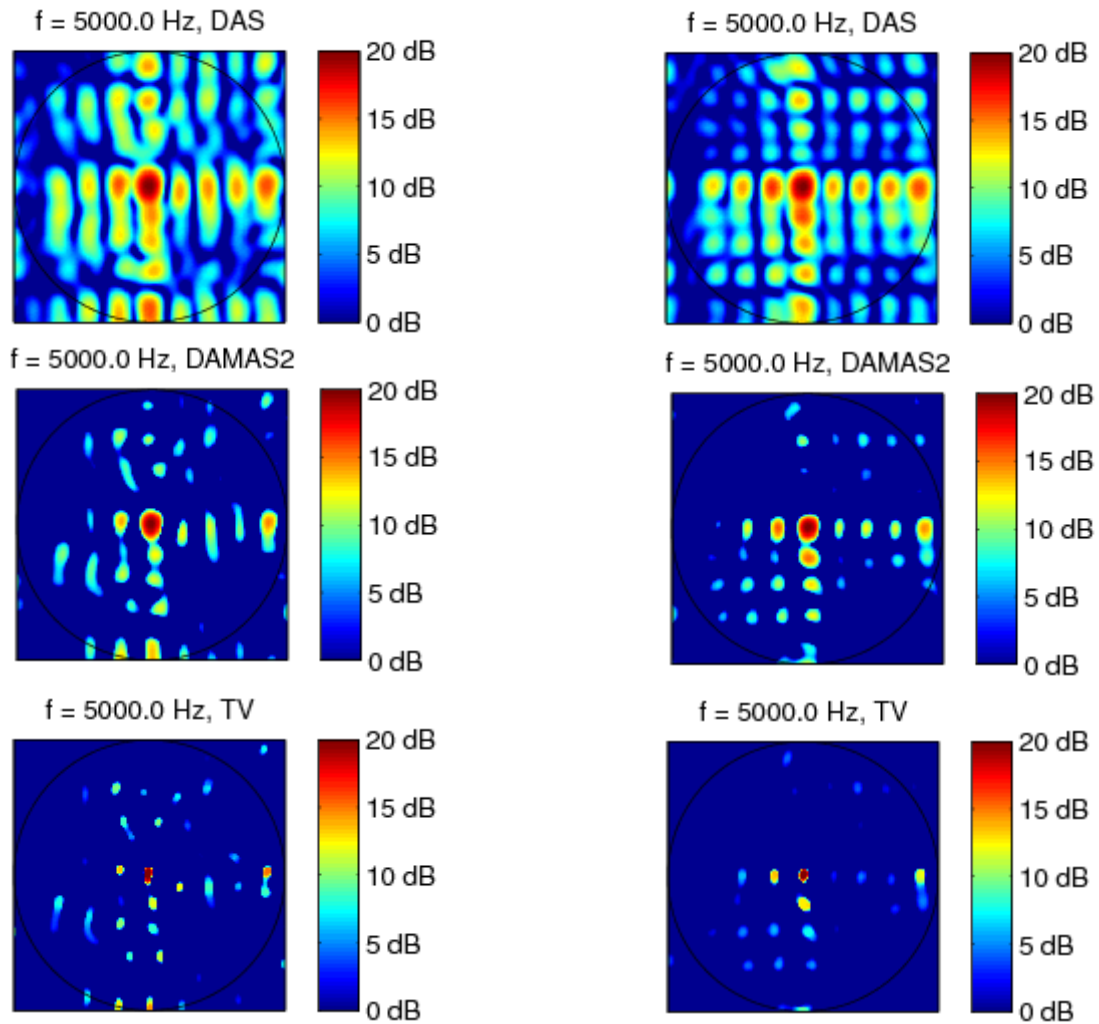


Figure 3. Acoustic images at 5 kHz obtained from microphone array measurements from a miniature loudspeaker positioned 1.5 m in front of the array calculated with DAS beamformer (1st line), DAMAS2 (2nd line), and TV regularized reconstruction (3rd line). First column shows reconstruction without calibration, and second column shows reconstruction with calibration.

6.2 One loudspeaker placed to the left of the microphone array

Figure 4 shows the image reconstruction of a sound source positioned 1.5 m in front and 0.65 m to the left of the center of the microphone array. The frequency used for reconstruction was 1,5 kHz. This example reinforces the drawbacks of DAS beamforming which produces smeared images with pronounced artifacts due to the sidelobes of the array's PSF. DAMAS2 and TV-regularization produces improved results, still, however, with the presence of artifacts, specially on the edges of the visible region. The source observed on the right side of the array is believed to be caused by the reflection of the sound wave at the glass window present on that side of the room.

Figure 5 presents image reconstruction for the same setup at a frequency of 5 kHz. Just as in the previous example, we now notice the increased presence of artifacts caused from the sidelobe of the PSF and that cannot be completely eliminated with the iterative imaging methods.

The ℓ_1 -regularized reconstruction algorithm did not converge to a solution and therefore is not depicted for this example.

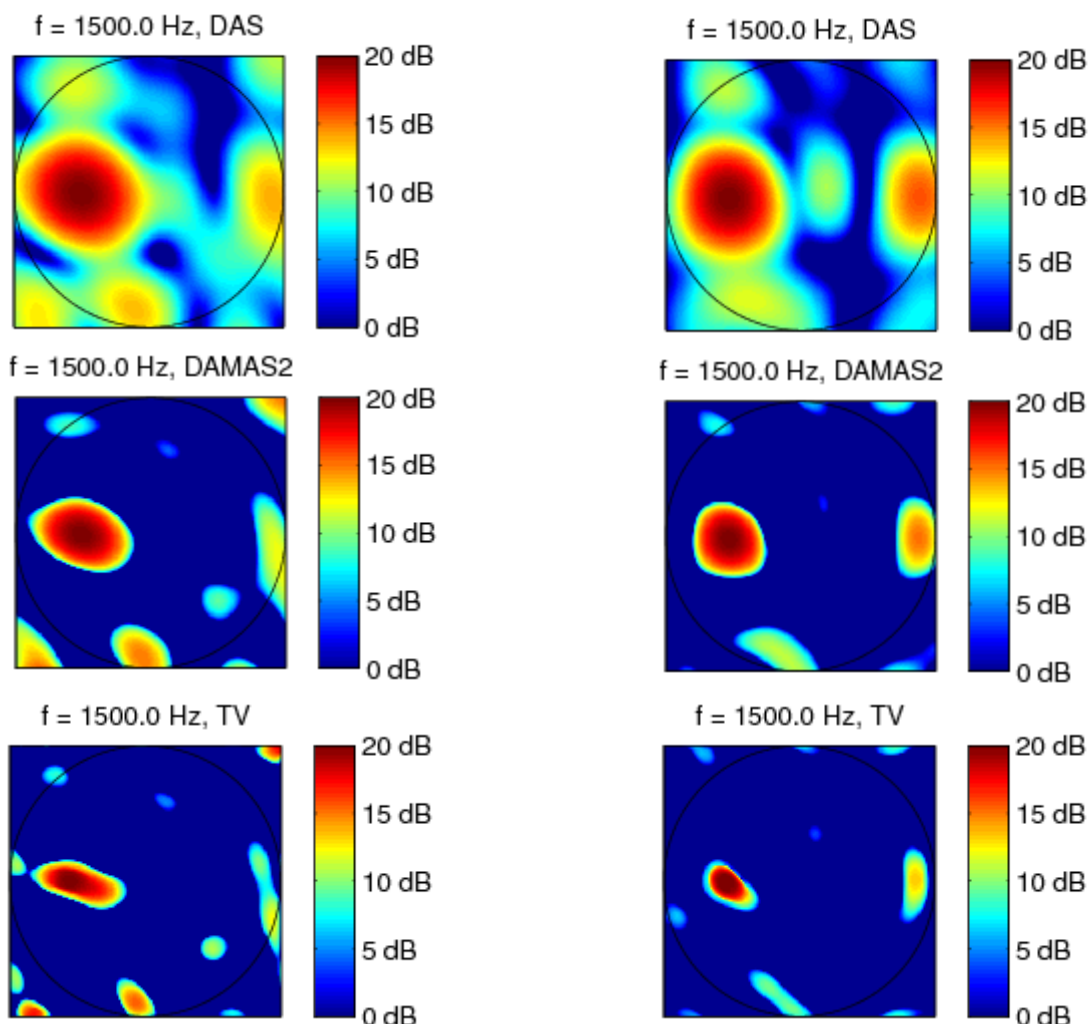


Figure 4. Acoustic images at 1.5 kHz obtained from microphone array measurements from a miniature loudspeaker positioned 1.5 m in front and 0.64 m to the left of the array calculated with DAS beamformer (1st line), DAMAS2 (2nd line), and TV regularized reconstruction (3rd line). First column shows reconstruction without calibration, and second column shows reconstruction with calibration.

6.3 Two loudspeakers placed 1.3 m apart from each other and in front of the microphone array

We now place two miniature loudspeakers positioned 1.5 m in front and 0.65 m to the left and 0.65 m to the right of the center of the microphone array. We now expect to see an image with the presence of two clear red regions in the otherwise blue background. Figure 6 shows the image reconstruction for the frequency of 1.5 kHz. DAS imaging identifies the location of the sources, but with the usual low quality of reconstruction. All other methods clearly detect the presence of two sources and the use of calibration provides significant reduction from artifacts. For this example ℓ_1 -regularized reconstruction provides a practically noise-free image.

Figure 7 presents reconstruction results for 5 kHz. In this case DAS result does not allow one to detect the presence of two sources, as the image of the actual source mixes with the sidelobe artifacts. Unfortunately the other imaging methods could not provide a better result for this setup, placing two sources at the right of the array instead of one left and one right as would be expected. We are still not aware of the causes for such behavior, that make it clear that there is more ground for research and improvement, first of all understanding the impact of the algorithm's parameters on the algorithm's results.

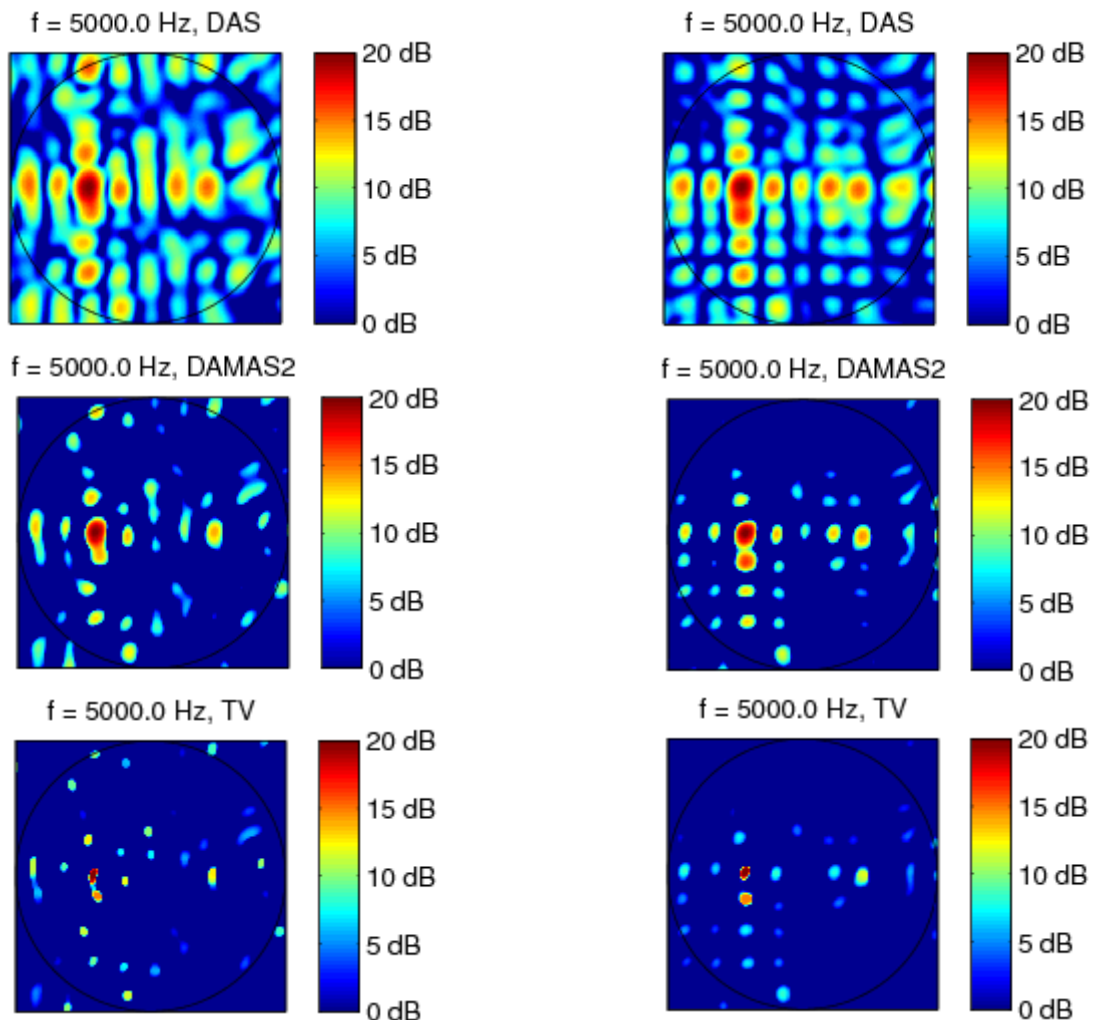


Figure 5. Acoustic images at 5 kHz obtained from microphone array measurements from a miniature loudspeaker positioned 1.5 m in front and 0.64 m to the left of the array calculated with DAS beamformer (1st line), DAMAS2 (2nd line), and TV regularized reconstruction (3rd line). First column shows reconstruction without calibration, and second column shows reconstruction with calibration.

7. CONCLUSION

In this paper we presented results of several acoustic image reconstructions obtained from measurements with a 49-microphone array and four different reconstruction methods: delay-and-sum beamforming, DAMAS2 and two forms of regularized least-squares, with and without calibration of the microphones. All computations were accelerated using the recently proposed Kronecker array transform.

In all experiments, results obtained with the regularized least-squares methods and DAMAS2 were superior to those obtained with beamforming. The use of microphone calibration also improved substantially the quality of the obtained images.

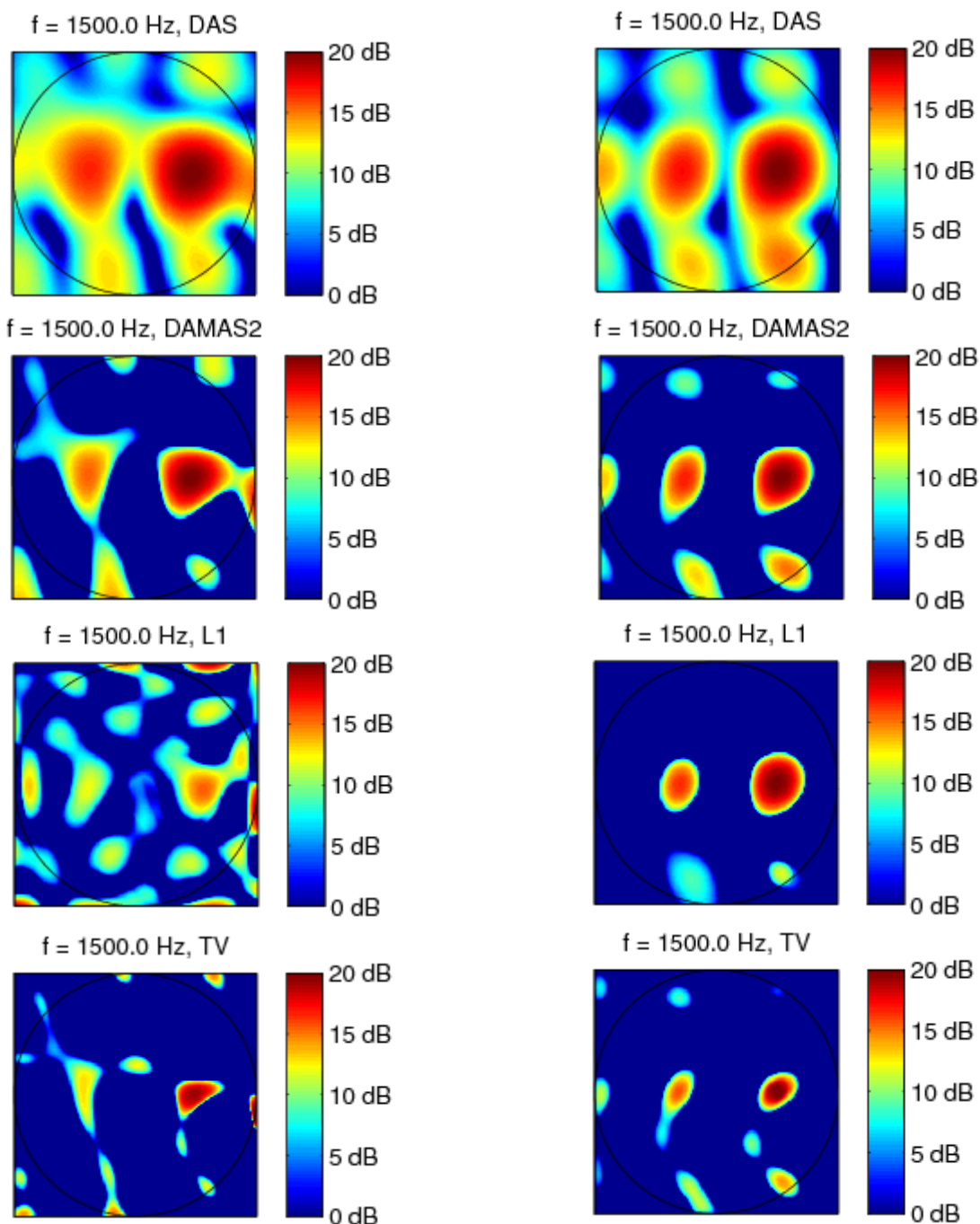


Figure 6. Acoustic images at 1.5 kHz obtained from microphone array measurements from two miniature loudspeaker positioned 1.5 m in front and 0.65 m to each side of the array calculated with DAS beamformer (1st line), DAMAS2 (2nd line), ℓ_1 -regularized reconstruction (3rd line), and TV regularized reconstruction (4th line). First column shows reconstruction without calibration, and second column shows reconstruction with calibration.

However, the obtained results were not satisfactory for all setups. It is now necessary to investigate the causes of this behavior as well as to understand the impact of the algorithm's parameters on the final result.

8. ACKNOWLEDGEMENTS

Bruno S. Masiero is grateful to FAPESP (Grant #14/06066-6) for financial support. Vítor H. Nascimento is grateful to FAPESP (Grant #14/04256-2) and CNPq (Grant #306268/2014-0) for partial financial support.

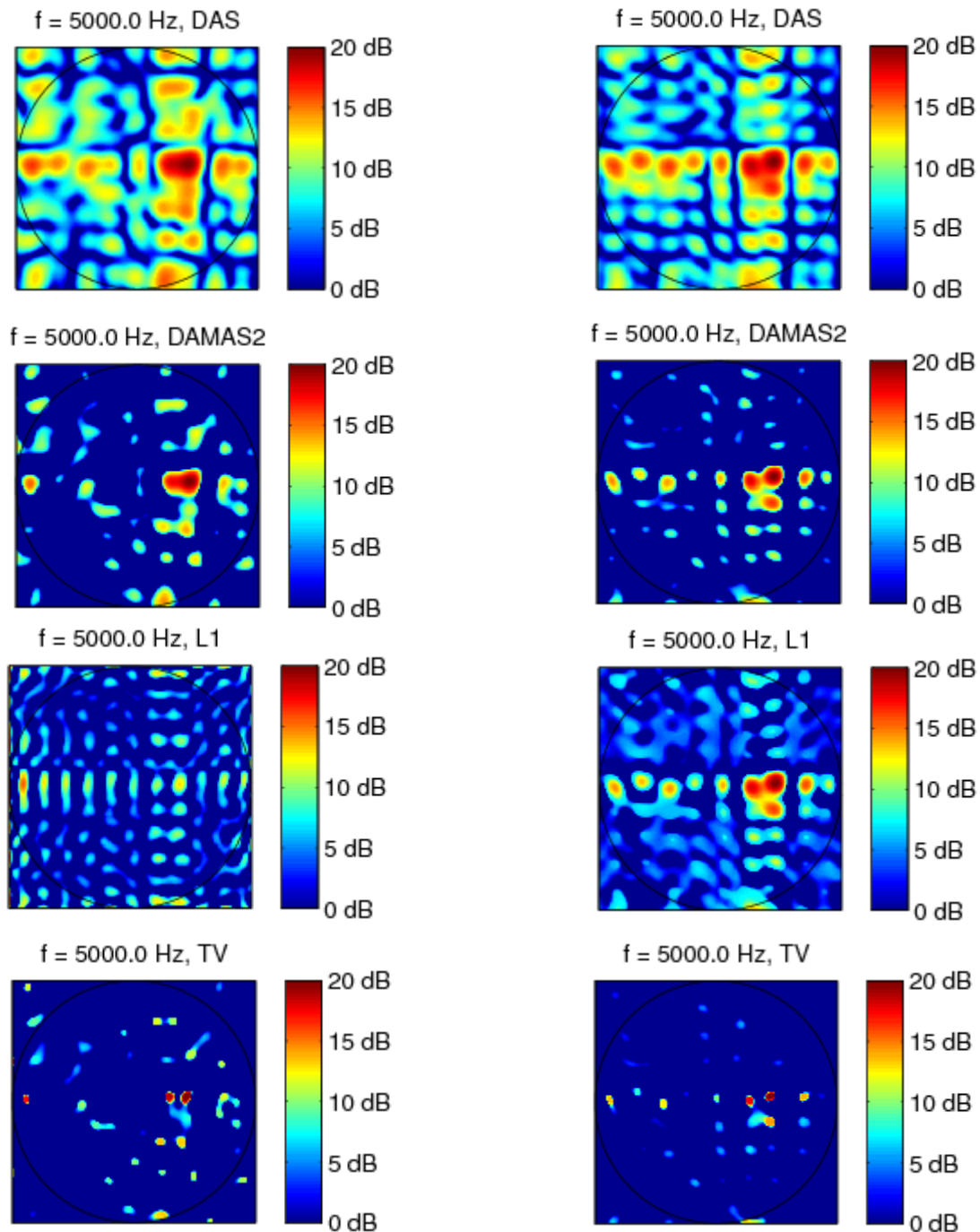


Figure 7. Acoustic images at 5 kHz obtained from microphone array measurements from two miniature loudspeaker positioned 1.5 m in front and 0.65 m to each side of the array calculated with DAS beamformer (1st line), DAMAS2 (2nd line), ℓ_1 -regularized reconstruction (3rd line), and TV regularized reconstruction (4th line). First column shows reconstruction without calibration, and second column shows reconstruction with calibration.

9. REFERENCES

- Van den Berg, E. and Friedlander, M.P., 2008. "Probing the Pareto Frontier for Basis Pursuit Solutions." *SIAM Journal on Scientific Computing*, 31(2), pp.890–912.
- Bouchard, M., Norcross, S.G. and Souloudre, G.A., 2006. "Inverse Filtering Design Using a Minimal-Phase Target Function from Regularization." In *121st AES Convention*. San Francisco, USA.
- Dietrich, P. et al., 2010. "MATLAB Toolbox for the Comprehension of Acoustic Measurement and Signal Processing." In *Fortschritte der Akustik -- DAGA*. Berlin, Germany, pp. 517–518.
- Dougherty, R.P., 2005. "Extensions of DAMAS and Benefits and Limitations of Deconvolution in Beamforming." In *11th AIAA/CEAS Aeroacoustics Conference*. pp. 1–13.
- Ehrenfried, K. and Koop, L., 2007. "Comparison of Iterative Deconvolution Algorithms for the Mapping of Acoustic Sources." *AIAA Journal*, 45(7), pp.1584–1595.
- Flanagan, B.P. and Bell, K.L., 2001. "Array self-calibration with large sensor position errors." *Signal Processing*, 81(10), pp.2201–2214.
- Johnson, D.H. and Dudgeon, D.E., 1993. *Array Signal Processing*, Prentice Hall, Englewood-Cliffs N.J.
- Khong, A.W.H. and Brookes, M., 2007. "The Effect of Calibration Errors on Source Localization with Microphone Arrays." In *2007 IEEE International Conference on Acoustics, Speech and Signal Processing - ICASSP '07*.
- Krim, H. and Viberg, M., 1996. "Two decades of array signal processing research: the parametric approach." *IEEE Signal Processing Magazine*, 13(4), pp.67–94.
- Li, C., 2009. *An Efficient Algorithm For Total Variation Regularization with Applications to the Single Pixel Camera*. Rice University.
- Ribeiro, F.P., 2012. *Arrays de Microfones para Medida de Campos Acústicos*. Universidade de São Paulo.
- Ribeiro, F.P. and Nascimento, V.H., 2011a. "Fast transforms for acoustic imaging- part I: Theory." *IEEE Transactions on Image Processing*, 20(8), pp.2229–2241.
- Ribeiro, F.P. and Nascimento, V.H., 2011b. "Fast transforms for acoustic imaging -part II: Applications." *IEEE Transactions on Image Processing*, 20(8), pp.2241–2247.
- Van Trees, H.L., 2002. *Optimum Array Processing: Part IV of Detection, Estimation and Modulation Theory*, John Wiley and Sons.
- Valente, S.D. et al., 2010. "Geometric calibration of distributed microphone arrays from acoustic source correspondences." *Multimedia Signal Processing (MMSP), 2010 IEEE International Workshop on*.
- Vertatschitsch, E. and Haykin, S., 1986. "Nonredundant arrays." *Proceedings of the IEEE*, 74, pp.217–217.
- Wang, Y. et al., 2004. "Wideband RELAX and wideband CLEAN for aeroacoustic imaging." *The Journal of the Acoustical Society of America*, 115, p.757.
- Weiss, A.J. and Friedlander, B., 1990. "Eigenstructure methods for direction finding with sensor gain and phase uncertainties." *Circuits, Systems, and Signal Processing*, 9, pp.271–300.
- Xiao, H., Shao, H. and Peng, Q., 2007. "A New Calibration Method for Microphone Array with Gain, Phase, and Position Errors." *JOURNAL OF ELECTRONIC SCIENCE AND TECHNOLOGY OF CHINA*, 5(3), pp.248–251.
- Yardibi, T. et al., 2008. "Sparsity constrained deconvolution approaches for acoustic source mapping." *The Journal of the Acoustical Society of America*, 123, p.2631.

10. RESPONSIBILITY NOTICE

The authors are the only responsible for the printed material included in this paper.